

2-2012

# Generalized ellipsometry in-situ quantification of organic adsorbate attachment within slanted columnar thin films

Keith B. Rodenhausen Jr.  
*University of Nebraska-Lincoln*, kbrod@engr.unl.edu

Daniel Schmidt  
*University of Nebraska-Lincoln*


Tadas Kasputis  
*University of Nebraska-Lincoln*, s-tkasput1@unl.edu

Angela K. Pannier  
*University of Nebraska-Lincoln*, apannier2@unl.edu

Eva Schubert  
*University of Nebraska-Lincoln*, efranke3@unl.edu

*See next page for additional authors*

Follow this and additional works at: <http://digitalcommons.unl.edu/chemengall>

 Part of the [Chemical Engineering Commons](#), [Engineering Science and Materials Commons](#), and the [Materials Science and Engineering Commons](#)

Rodenhausen, Keith B. Jr.; Schmidt, Daniel; Kasputis, Tadas; Pannier, Angela K.; Schubert, Eva; and Schubert, Mathias, "Generalized ellipsometry in-situ quantification of organic adsorbate attachment within slanted columnar thin films" (2012). *Chemical and Biomolecular Engineering -- All Faculty Papers*. 1.  
<http://digitalcommons.unl.edu/chemengall/1>

This Article is brought to you for free and open access by the Chemical and Biomolecular Engineering, Department of at DigitalCommons@University of Nebraska - Lincoln. It has been accepted for inclusion in Chemical and Biomolecular Engineering -- All Faculty Papers by an authorized administrator of DigitalCommons@University of Nebraska - Lincoln.

---

**Authors**

Keith B. Rodenhausen Jr., Daniel Schmidt, Tadas Kasputis, Angela K. Pannier, Eva Schubert, and Mathias Schubert

# Generalized ellipsometry *in-situ* quantification of organic adsorbate attachment within slanted columnar thin films

Keith B. Rodenhause<sup>1,\*</sup> Daniel Schmidt,<sup>2</sup> Tadas Kasputis,<sup>3</sup> Angela  
K. Pannier,<sup>3</sup> Eva Schubert,<sup>2</sup> and Mathias Schubert<sup>2</sup>

<sup>1</sup>Department of Chemical and Biomolecular Engineering, University of Nebraska-Lincoln,  
207 Othmer Hall, Lincoln, NE 68588, USA

<sup>2</sup>Department of Electrical Engineering, University of Nebraska-Lincoln,  
209N Scott Engineering Center, Lincoln, NE 68588, USA

<sup>3</sup>Department of Biological Systems Engineering, University of Nebraska-Lincoln,  
223 L. W. Chase Hall, East Campus, Lincoln, NE 68583, USA

\*kbrod@engr.unl.edu

**Abstract:** We apply generalized ellipsometry, well-known to be sensitive to the optical properties of anisotropic materials, to determine the amount of fibronectin protein that adsorbs onto a Ti slanted columnar thin film from solution. We find that the anisotropic optical properties of the thin film change upon organic adsorption. An optical model for ellipsometry data analysis incorporates an anisotropic Bruggeman effective medium approximation. We find that differences in experimental data from before and after fibronectin adsorption can be solely attributable to the uptake of fibronectin within the slanted columnar thin film. Simultaneous, *in-situ* generalized ellipsometry and quartz crystal microbalance measurements show excellent agreement on the amount and rate of fibronectin adsorption. Quantitative characterization of organic materials within three-dimensional, optically anisotropic slanted columnar thin films could permit their use in optical sensor applications.

© 2012 Optical Society of America

**OCIS codes:** (240.2130) Ellipsometry and polarimetry.

---

## References and links

1. W. Yang, J. Y. Gerasimov, and R. Y. Lai, "Folding-based electrochemical DNA sensor fabricated on a gold-plated screen-printed carbon electrode," *Chem. Commun.* **20**, 2902–2904 (2009).
2. R. M. Burks, S. E. Pacquette, M. A. Guericke, M. V. Wilson, D. J. Symonsbergen, K. A. Lucas, and A. E. Holmes, "DETECHIP®: a sensor for drugs of abuse," *J. Forensic Sci.* **55**, 723–727 (2010).
3. K. Robbie and M. J. Brett, "Sculptured thin films and glancing angle deposition: growth mechanics and applications," *J. Vac. Sci. Technol. A* **15**, 1460–1465 (1997).
4. D. Schmidt, E. Schubert, and M. Schubert, "Generalized ellipsometry determination of non-reciprocity in chiral silicon sculptured thin films," *Phys. Stat. Sol. A* **205**, 748–751 (2008).
5. D. Schmidt, A. C. Kjerstad, T. Hofmann, R. Skomski, E. Schubert, and M. Schubert, "Optical, structural, and magnetic properties of cobalt nanostructure thin films," *J. Appl. Phys.* **105**, 113508 (2009).
6. D. Schmidt, B. Booso, T. Hofmann, E. Schubert, A. Sarangan, and M. Schubert, "Monoclinic optical constants, birefringence, and dichroism of slanted titanium nanocolumns determined by generalized ellipsometry," *Appl. Phys. Lett.* **94**, 011914 (2009).
7. D. Schmidt, C. Müller, T. Hofmann, O. Inganäs, H. Arwin, E. Schubert, and M. Schubert, "Optical properties of hybrid titanium chevron sculptured thin films coated with a semiconducting polymer," *Thin Solid Films* **519**, 2645–2649 (2009).

8. D. van Noort and C.-F. Mandenius, "Porous gold surfaces for biosensor applications," *Biosens. Bioelectron.* **15**, 203–209 (2000).
9. F. Höök, B. Kasemo, T. Nylander, C. Fant, K. Sott, and H. Elwing, "Variations in coupled water, viscoelastic properties, and film thickness of a mefp-1 protein film during adsorption and cross-linking: a quartz crystal microbalance with dissipation monitoring, ellipsometry, and surface plasmon resonance study," *Anal. Chem.* **73**, 5796–5804 (2001).
10. E. Bittrich, K. B. Rodenhausen, K.-J. Eichhorn, T. Hofmann, M. Schubert, M. Stamm, and P. Uhlmann, "Protein adsorption on and swelling of polyelectrolyte brushes: a simultaneous ellipsometry-quartz crystal microbalance study," *Biointerphases* **5**, 1–9 (2010).
11. R. A. May, D. W. Flaherty, C. B. Mullins, and K. J. Stevenson, "Hybrid generalized ellipsometry and quartz crystal microbalance nanogravimetry for the determination of adsorption isotherms on biaxial metal oxide films," *J. Phys. Chem. Lett.* **1**, 1264–1268 (2010).
12. K. B. Rodenhausen, T. Kasputis, A. K. Pannier, J. Y. Gerasimov, R. Y. Lai, M. Solinksy, T. Tiwald, A. Sarkar, T. Hofmann, N. Ianno, and M. Schubert, "Combined optical and acoustical method for determination of thickness and porosity of transparent organic layers below the ultra-thin film limit," *Rev. Sci. Instrum.* **82**, 103111 (2011).
13. D. A. G. Bruggeman, "Berechnung verschiedener physikalischer konstanten von heterogenen substanzen. I. dielektrizitätskonstanten und leitfähigkeiten der mischkörper aus isotropen substanzen," *Ann. Phys.* **416**, 636–679 (1935).
14. D. Polder and J. H. van Santen, "The effective permeability of mixtures of solids," *Physica* **12**, 257–271 (1946).
15. D. Schmidt, E. Schubert, and M. Schubert, "Optical properties of cobalt sculptured thin films passivated by atomic layer deposition," *Appl. Phys. Lett.* **100**, 011912 (2012).
16. C. G. Granqvist, D. L. Bellac, and G. A. Niklasson, "Angular selective window coatings: effective medium theory and experimental data on sputter-deposited films," *Renew. Energ.* **8**, 530–539 (1996).
17. H. P. Erickson, "Size and shape of protein molecules at the nanometer level determined by sedimentation, gel filtration, and electron microscopy," *Biol. Proced. Online* **11**, 32–51 (2009).
18. T. Berlind, G. K. Pribil, D. Thompson, J. A. Woollam, and H. Arwin, "Effects of ion concentration on refractive indices of fluids measured by the minimum deviation technique," *Phys. Stat. Sol. C* **5**, 1249–1252 (2008).
19. D. Schmidt, B. Booso, T. Hofmann, E. Schubert, A. Sarangan, and M. Schubert, "Generalized ellipsometry for monoclinic absorbing materials: determination of optical constants of Cr columnar thin films," *Opt. Lett.* **34**, 992–994 (2009).
20. G. Sauerbrey, "Verwendung von schwingquarzen zur wägung dünner schichten und zur mikrowägung," *Z. Phys. A-Hadron Nucl.* **155**, 206–222 (1959).
21. B. Ivarsson and I. Lundström, "Physical characterization of protein adsorption on metal and metal oxide surfaces," *Crit. Rev. Biocompat.* **2**, 1–96 (1986).
22. M. B. Hovgaard, K. Rechendorff, J. Chevallier, M. Foss, and F. Besenbacher, "Fibronectin adsorption on tantalum: the influence of nanoroughness," *J. Phys. Chem. B* **112**, 8241–8249 (2008).

---

## 1. Introduction

Optical sensor technologies are being developed to detect the presence of analytes including specific deoxyribonucleic acid (DNA) sequences [1] and contraband [2]. An optical approach can provide the benefits of contactless, non-destructive measurement. Slanted columnar thin films (SCTFs) produced by electron-beam glancing angle deposition (GLAD) [3] are promising scaffolding materials for such sensors. A SCTF is a layer of nanocolumns that are tilted at a slanting angle. SCTFs have optically anisotropic properties and offer increased surface area for analyte attachment. Many applications necessitate real-time *in-situ* measurements under native liquid ambient. Analytes may degrade or change their conformation upon exposure to an air or vacuum environment.

It has been previously shown [4–7] that generalized ellipsometry (GE) is extremely sensitive to the anisotropic properties of SCTFs. In this work, GE measurements include the determination of select Mueller matrix element spectra. GE measurements detect, as a new working principle for organic adsorbate detection, changes in birefringence of the SCTF materials rather than changes in effective refractive indices, as reported, for example, for randomly porous, and therefore optically isotropic, sensing surfaces [8]. The advantage of increased surface area in randomly porous surfaces for optical sensing of analyte attachment is preserved for the SCTF analogue because three-dimensional surfaces also possess an increased surface area with respect to a flat substrate. The quartz crystal microbalance with dissipation (QCM-

D) technique has been used to monitor protein adsorption and cross-linking [9] and polyelectrolyte brush swelling [10] and is used as a reference method here. Recently, May *et al.* demonstrated the use of GE to measure vapor-phase adsorption isotherms of toluene onto transparent TiO<sub>2</sub> slanted SCTFs and corroborated the result with simultaneous quartz crystal microbalance (QCM) measurements [11].

We demonstrate the use of GE to determine changes of the anisotropic properties of SCTFs upon organic analyte adsorption from solution; GE allows the quantification of the amount of analyte that adsorbs into the void spaces of a SCTF. We perform *in-situ* GE measurements on a Ti SCTF during human plasma fibronectin protein (FN) adsorption within a liquid environment. Simultaneous QCM-D measurements are performed for comparison. As commonly observed, assumptions of the analyte index of refraction and density are required [12]. We demonstrate excellent agreement between GE and QCM-D results for the amount and rate of FN adsorption.

## 2. Theory

### 2.1. Anisotropic Bruggeman effective medium approximation

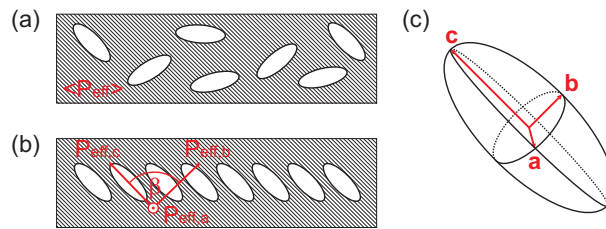


Fig. 1. Effective medium scenarios with mixtures of ellipsoidal inclusions (general case) and a homogeneous host matrix. The mixture with randomly oriented inclusions (a) exhibits an average effective polarizability  $\langle \mathbf{P}_{\text{eff}} \rangle$  whereas the mixture with aligned inclusions (b) shows anisotropic properties with three effective polarizability components  $\mathbf{P}_{\text{eff},j}$ . The major polarizability axes system rendering the biaxial nature of the film is depicted in (c).

Volume fractions of a multiple-component layer can be determined from ellipsometry measurements through an effective medium approximation (EMA). A Bruggeman EMA renders the polarizabilities of constituent materials as equivalent spherical inclusions within a host matrix to determine an effective dielectric function [13]. Anisotropic inclusions can be modeled in an EMA by introducing depolarization factors  $L_j^D$  ( $j = a, b, c$ ) along each of the three orthogonal, major optical polarizability axes (**a**, **b**, and **c**), such that the polarizability-describing inclusions become ellipsoidal [14]. Figure 1(a) shows an effectively isotropic mixture with an average effective polarizability  $\langle \mathbf{P}_{\text{eff}} \rangle$  due to the random orientations of the ellipsoidal inclusions in the host matrix. In Fig. 1(b), the ellipsoidal inclusions are aligned and exhibit anisotropic properties with three effective polarizability components  $\mathbf{P}_{\text{eff},j}$ . Instead of one “isotropic” effective dielectric function averaged over all major polarizability axes, three effective dielectric function components averaged over their individual axes are acquired. Thus, Mueller matrix spectra of organic materials within an anisotropic SCTF under a liquid ambient can be described by an optical model that includes an anisotropic Bruggeman effective medium approximation (AB-EMA). Multiple components of a layer described by an AB-EMA model can be determined via GE analysis [15]. Given the constraint that the sum of all volume fractions  $f_n$  must equal unity, the AB-EMA equations for  $m$  constituent materials are

$$\sum_{n=1}^m f_n \frac{\epsilon_n - \epsilon_{\text{eff},j}}{\epsilon_{\text{eff},j} + L_j^D (\epsilon_n - \epsilon_{\text{eff},j})} = 0, \quad (1)$$

where  $\epsilon_{\text{eff},j}$  is the effective dielectric function along the  $j$ th axis and  $\epsilon_n$  is the bulk dielectric function of the  $n$ th constituent material [16]. In this analysis it is necessary to assume a certain value for the complex index of refraction ( $\epsilon = N^2$ ) of FN, which is set to 1.5 [12].

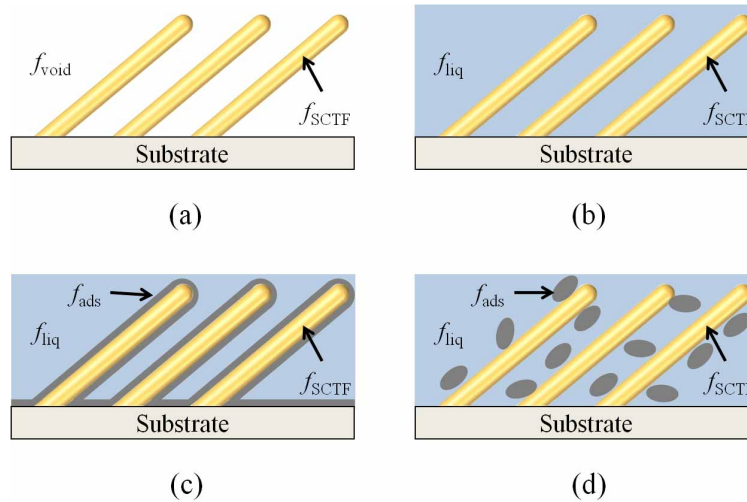


Fig. 2. Illustrations of constituent material fraction regimes. (a) represents a SCTF ( $f_{\text{SCTF}}$ ) in air ( $f_{\text{void}}$ ) ambient. (b) applies after liquid ( $f_{\text{liq}}$ ) replaces air as the ambient, and  $f_{\text{liq}} = f_{\text{void}}$ . (c) and (d) represent arrangements of material after an identical amount of analyte ( $f_{\text{ads}}$ ) adsorbs and displaces liquid ambient, and  $f_{\text{liq}} + f_{\text{ads}} = f_{\text{void}}$ .

Figure 2 shows how fraction parameters represent sample volume spaces. In air ambient [Fig. 2(a)],  $f_{\text{SCTF}}$  and  $f_{\text{void}}$  represent the SCTF and air contributions, respectively. After liquid introduction [Fig. 2(b)], void spaces are filled by liquid ( $f_{\text{liq}}$ ), such that  $f_{\text{liq}} = f_{\text{void}}$ . Upon analyte adsorption [Figs. 2(c) and 2(d)], some liquid is replaced by analyte ( $f_{\text{ads}}$ ), and  $f_{\text{liq}} + f_{\text{ads}} = f_{\text{void}}$ . Figures 2(c) and 2(d) represent alternative arrangements of constituent liquid and ambient material. In a strict sense, the AB-EMA is consistent with scenarios depicted by Figs. 2(a)-2(c), as all components have the same shape implied by common depolarization factors  $L_j^D$ . The scenario represented by Fig. 2(d) is meant to address situations where the FN is attached to the SCTF surface and is detectable by QCM-D. Further refinement of the AB-EMA model descriptions are needed to include and potentially differentiate between scenarios depicted by Figs. 2(c) and 2(d). The AB-EMA fraction parameters in the optical model are varied while experimental and model-generated data are matched to reflect these composition changes during a dynamic adsorption process.

Surface mass density parameters are found to directly compare the amount of adsorbate that GE and QCM-D detect. As will be shown in Sec. 2.3, a surface mass density parameter is immediately yielded by the QCM-D analysis. The thickness of the AB-EMA model layer is equivalent to the SCTF thickness  $d_{\text{SCTF}}$  and can be extracted from the optical model. An optical surface density  $\Gamma_{\text{GE}}$  is obtained via the following equation:

$$\Gamma_{\text{GE}} = \rho_{\text{ads}} f_{\text{ads}} d_{\text{SCTF}}, \quad (2)$$

where  $\rho_{\text{ads}}$  is the density of adsorbate, which we assume to be 1.37 g/mL for proteins such as FN [17]. Note that the surface density parameters are calculated as though they are over flat reference areas.

## 2.2. Generalized ellipsometry optical model

A stratified three-layer optical model is used to represent the experimental system. A Au-coated QCM-D sensor is described by a substrate model layer; the dielectric function of the substrate was determined prior to this investigation. The SCTF with ambient and organic adsorbate inclusions is described by an AB-EMA model layer. The AB-EMA model layer comprises the following components: ambient inclusions, SCTF material, and organic adsorbate. Finally, an isotropic organic model layer on top of the AB-EMA model layer is considered. Two different locations of organic adsorption, within and on top of the SCTF, are thereby considered. For a dynamic GE experiment (comprising multiple data sets over time) where ambient materials are exchanged, the index of refraction variation of the ambient material in the optical model must be considered. The optical constants of the varied ambient materials are measured by the minimum deviation technique prior to the *in-situ* data analysis [18]. Window effects in the form of an ellipsometric parameter  $\Delta$  offset are taken into account when a liquid cell is employed [12].

The liquid cell limits the experiment to one configuration of the sample in-plane azimuth angle and the angle of incidence. A configuration addresses a given sample in-plane azimuth angle, between the SCTF slanting direction and the plane of incidence, and a given angle of incidence. We described previously that metal SCTFs behave as effectively monoclinic thin films with monoclinic parameter  $\beta$  [5, 6].

To develop the optical model, a sequence of GE measurements is taken. After each measurement, relevant parameters in the optical model are varied while model-generated and experimental data sets are matched. First, a measurement is taken of the SCTF in open air at many configurations, as described in Refs. [6, 19]. The varied model parameters are (a) the amplitudes, critical-point transition energies, and broadening parameters of four Lorentzian oscillators for the Ti composing the SCTF in the AB-EMA model layer, (b) the AB-EMA model layer thickness, (c)  $f_{\text{void}}$  ( $f_{\text{SCTF}} = 1 - f_{\text{void}}$  while  $f_{\text{ads}}$  is set to zero), (d) the depolarization factors  $L_j^D$ , (e) the SCTF slanting angle  $\theta$ , (f) the SCTF in-plane azimuth angle, and (g) the monoclinic parameter  $\beta$ . Second, a measurement is taken of the SCTF in open air at the configuration it would be after placement inside the liquid cell. The same model parameters (a)-(g) are varied during model-calculated and experimental data matching. Third, a measurement is taken after the sample is placed in the liquid cell; from this point, measurements are only taken at this experimental configuration. (f) and (h) the  $\Delta$  offset are varied during model-calculated and experimental data matching. Fourth, a measurement is taken after liquid ambient replaced air in the liquid cell. The optical constants of air are replaced by those of the liquid ambient material in the model, and  $\beta$  is set to  $90^\circ$ . (a) and (d) are varied during model-calculated and experimental data matching. Then the organic adsorption experiment is performed. Thus, fifth, a series of measurements is taken during the organic adsorption process. The optical constants of the liquid ambient in the model are exchanged to those of the liquid ambient with the dissolved organic adsorbate. (i)  $f_{\text{ads}}$  ( $f_{\text{liq}} = 1 - f_{\text{ads}} - f_{\text{SCTF}}$  while  $f_{\text{SCTF}}$  is held constant) and (j) the thickness of the isotropic organic model layer are varied during model-calculated and experimental data matching. The starting value for  $f_{\text{liq}}$  is  $f_{\text{void}}$ .

## 2.3. Quartz crystal microbalance with dissipation

QCM is a mechanical technique whereby the mass of material that adsorbs onto an oscillating piezoelectric material, *e.g.*, quartz, is determined by measuring shifts in shear-mode vibrational frequency overtones. For adsorbate materials that can be assumed rigid, the Sauerbrey equation [20] provides a linear relationship between frequency shifts and mass attachment or loss, such that



$$\Gamma_{\text{QCM}} = -\frac{\delta v_{N_{\text{ov}}} \sqrt{\rho_{\text{q}} \mu_{\text{q}}}}{2v_0^2 N_{\text{ov}}}, \quad (3)$$

where  $\Gamma_{\text{QCM}}$  is the shift in attached mass per unit area,  $v_0$  is the fundamental frequency,  $\delta v_{N_{\text{ov}}}$  is the frequency shift of overtone  $N_{\text{ov}} = 3, 5, \dots$ ,  $\rho_{\text{q}}$  is the density of quartz, and  $\mu_{\text{q}}$  is the shear modulus of quartz. QCM-D additionally measures a frequency dissipation parameter that signifies the degree of viscoelasticity that the experimental system exhibits.

### 3. Materials and methods

Slanted Ti nanocolumns were deposited onto a gold-coated QCM sensor via GLAD as described elsewhere [3–6]. *Ex-situ* Mueller matrix spectra for the SCTF sample were acquired with a spectroscopic ellipsometer (M2000VI, J.A. Woollam Co., Inc.) from the wavelength range of 400 to 1000 nm. Measurements proceeded along  $6^\circ$  increments of sample rotation ( $0^\circ$  to  $360^\circ$ ). At each rotation interval, four measurements in  $10^\circ$  angle-of-incidence increments ( $45^\circ$  to  $75^\circ$ ) were taken.

*In-situ* GE measurements of approximately 1 min in duration were taken in a liquid cell for combinatorial ellipsometry and QCM-D (Ellipsometry module, E1 QCM-D, Biolin Scientific) measurements [12]; the sample in-plane azimuth angle was fixed at  $90^\circ$ , such that slanted columns were oriented normal to the ellipsometry plane of incidence, and the liquid cell had a  $65^\circ$  angle of incidence. As explained in Section 2.2, two GE measurements (one at many configurations, the second at only the *in-situ* configuration) were acquired in air to characterize the SCTF.

10  $\mu\text{g/mL}$  FN (Sigma-Aldrich, St. Louis, MO) solution was prepared in standard 1X phosphate-buffered saline (PBS) at pH 7.4 (Invitrogen, Carlsbad, CA); no other additives were included. The optical constants of PBS-only and FN solutions were experimentally determined by the minimum deviation technique. The sample was then loaded into the liquid cell, and another GE measurement was taken to account for window effects. Similarly, a GE measurement was taken while PBS-only solution was pumped through the liquid cell at a constant rate of 0.1 mL/min to account for the change of ambient. At this point, the necessary measurements for building the optical model were complete. GE measurements continued to be taken, and a dynamic QCM-D measurement was started. After signal baselines were reached ( $t = 147$  min), FN solution was introduced into the liquid cell at the same flow rate. 35 min later ( $t = 182$  min), PBS-only solution was directed into the cell to rinse passively adsorbed and freely floating FN. GE measurements were taken throughout the adsorption and rinsing processes. Note that the optical constants of the ambient material in the optical model were exchanged between PBS-only solution and FN solution to reflect which ambient was currently flowing into the liquid cell. Details of the combinatorial ellipsometry and QCM-D module and technique were recently presented [12].

### 4. Results and discussion

*In-situ* experimental Mueller matrix element spectra that reveal sensitivity to the presence of FN are shown in Fig. 3. The spectra are from data sets taken before ( $t = 145$  min) and after ( $t = 220$  min) the FN adsorption and rinsing processes. The Mueller matrix element spectra featured in Fig. 3 were chosen because we found them to be most responsive to FN adsorption. The best-match model-generated data for the experimental GE data taken after the PBS rinse ( $t = 220$  min) is shown in Fig. 4. Matching experimental and model-generated data sets yielded zero thickness for the isotropic FN model layer on top of the AB-EMA model layer. Therefore, all differences between experimental data in Fig. 3 are explained by the optical model as solely due to the increase of  $f_{\text{ads}}$  at the expense of  $f_{\text{liq}}$  in the AB-EMA model layer.



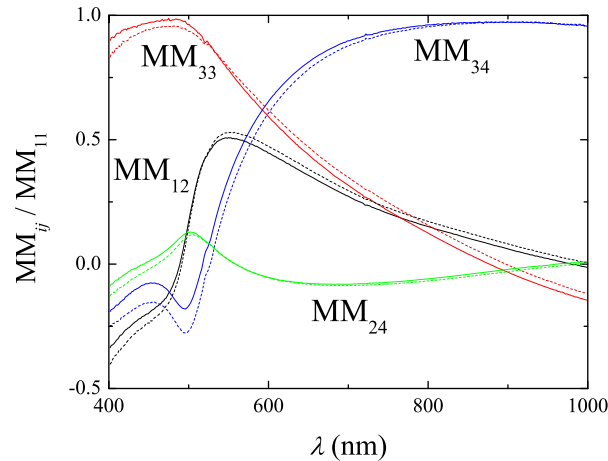


Fig. 3. Select experimental Mueller matrix element spectra from GE measurements just before the FN introduction (solid lines) at  $t = 145$  min and after FN adsorption and the PBS rinse (dotted lines) at  $t = 220$  min.

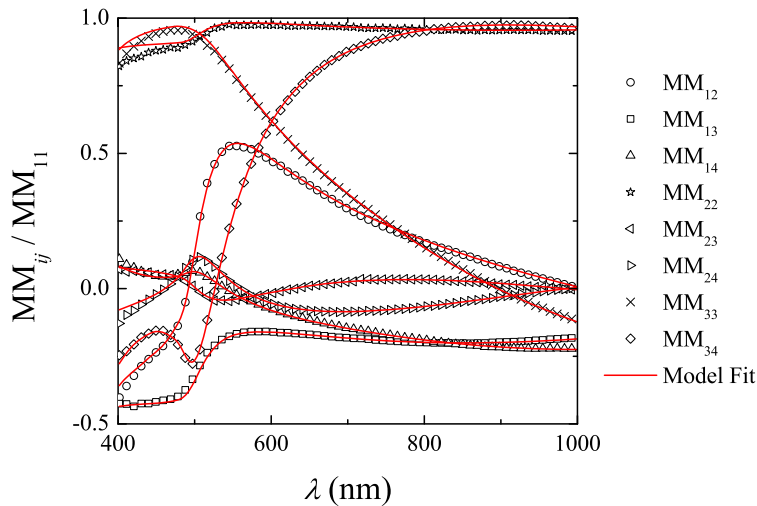


Fig. 4. Model-generated (lines) and reduced experimental (symbols) Mueller matrix element spectra after FN adsorption and the PBS rinse at  $t = 220$  min. Elements  $MM_{21}$ ,  $MM_{31}$ , and  $MM_{32}$  are omitted due to significant overlap with elements  $MM_{12}$ ,  $MM_{13}$ , and  $MM_{23}$ , respectively.

$\Gamma_{GE}$  was determined via the AB-EMA model layer thickness and fraction parameters from the optical model and Eq. (2). From the optical model,  $d_{SCTF} = 103$  nm,  $f_{SCTF} = 0.184$ , and  $\theta = 59^\circ$ . From SEM micrographs of other prepared Ti SCTFs, we estimate the column radius to be 12 nm. With these values, we can roughly estimate a column length of 193 nm, the number of columns per square  $\mu\text{m}$  to be 218, the distance between adjacent columns to be 68 nm, and the ratio of the SCTF surface area to a flat reference area to be 4.2. If approximately  $2 \text{ mg/m}^2$  of dry FN adsorbs onto a flat Ti surface [21], the geometry estimation yields a FN surface density of  $8.4 \text{ mg/m}^2$  on the SCTF. This is close to our reported value of  $14.3 \text{ mg/m}^2$  from GE (after

PBS rinsing). The SCTF surface area could be higher due to surface roughness generated by the GLAD process.

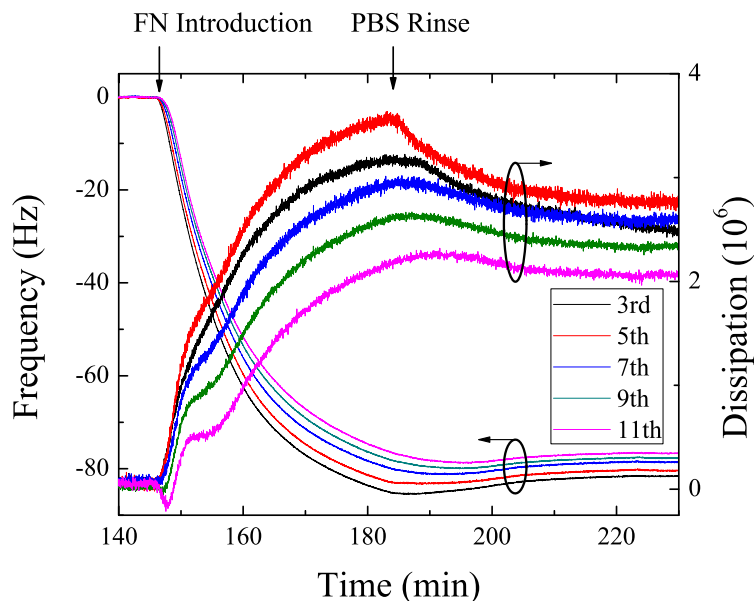


Fig. 5. QCM-D frequency (left axis) and dissipation (right axis) data for all experimental overtones ( $N_{ov} = 3, 5, \dots, 11$ ) during FN adsorption and PBS rinsing. Frequency overtones are normalized by overtone number. FN solution is introduced at  $t = 147$  min, and rinsing begins at  $t = 182$  min.

The raw QCM-D data for all experimental overtones ( $N_{ov} = 3, 5, \dots, 11$ ) is shown in Fig. 5. Aside from a shoulder in the dissipation curves at  $t = 150$  min, Fig. 5 shows similar frequency and dissipation values as seen for FN adsorption on flat Ta by Hovgaard *et al.* We consider the similarity noteworthy because the surface geometries are significantly different between the experiments. The dissipation shifts are very small compared to the frequency shifts, and as Hovgaard *et al.* did, we assume a rigid FN layer [22]. Equation (3) was applied to the third harmonic overtone to yield  $\Gamma_{QCM}$  over a reference flat surface.

The dynamic results of the QCM-D and GE analyses are shown in Fig. 6. FN adsorption and PBS rinsing processes begin at approximately  $t = 147$  min and  $t = 182$  min, respectively. The shifts of  $\Gamma_{GE}$  and  $\Gamma_{QCM}$  closely mirror each other. At  $t = 220$  min, after the PBS rinse, the GE and QCM-D surface density values are approximately  $14.3 \text{ mg/m}^2$  and  $14.1 \text{ mg/m}^2$ , respectively. In contrast, Hovgaard *et al.* reported an ellipsometry-derived surface density of approximately  $2 \text{ mg/m}^2$ ; their result is in agreement with a null ellipsometry experiment by Ivarsson and Lundström for FN adsorption onto flat Ti [21, 22].

Usually  $\Gamma_{QCM}$  is larger than  $\Gamma_{GE}$  due to the inclusion of mechanically coupled water in  $\Gamma_{QCM}$  [9, 12, 22]. If we assume that water in the void spaces of the SCTF is rigidly coupled to the Ti columns prior to FN adsorption,  $\Gamma_{QCM}$  is the difference of mass between an equivalent volume of FN ( $\rho_{ads} = 1.37 \text{ g/mL}$ ) and displaced water ( $\rho_{liq} = 1 \text{ g/mL}$ ). This assumption is incompatible with the GE results, as  $\Gamma_{QCM}$  would have to be much smaller than  $\Gamma_{GE}$ , which is only the mass of adsorbed FN. Similar  $\Gamma_{QCM}$  and  $\Gamma_{GE}$  values imply that water is not mechanically bound to the FN or the SCTF and that FN takes a different conformation on the SCTF surface compared to a flat surface. The implemented AB-EMA model layer does not differentiate between scenarios

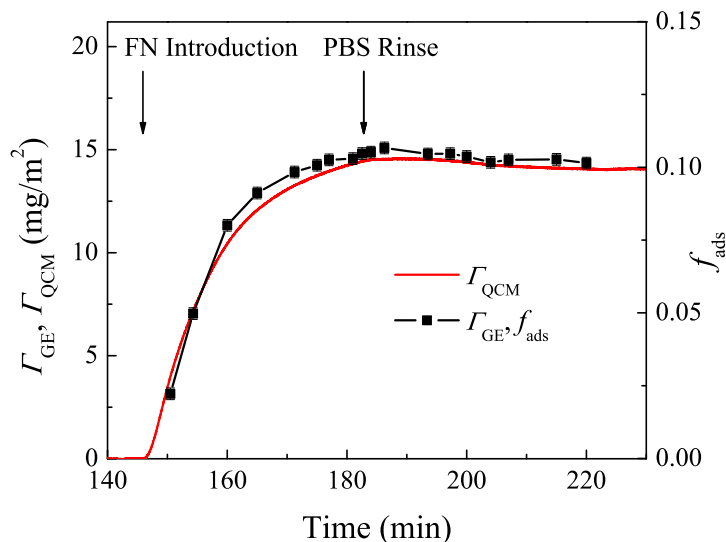


Fig. 6. Surface density and volumetric fraction parameters during FN adsorption and PBS rinsing. FN solution is introduced at  $t = 147$  min, and rinsing begins at  $t = 182$  min.  $f_{\text{ads}}$  and its error bars (in many cases overlapped by data points due to small error) are taken directly from the results of the AB-EMA model.

depicted in Figs. 2(c) and 2(d). Future work should address the refinement of QCM-D modeling approaches because the currently employed model system, the Sauerbrey equation, at this point, can only serve as an estimate for three-dimensional surfaces. A benefit of such work would be the potential for QCM-D to discern between these two scenarios. Nevertheless, the qualitative agreement between GE and QCM-D is excellent.

The error bar shown for the GE results in Fig. 6 appropriately takes into account the systematic and random error sources, which are cast into the data uncertainties and propagate through the numerical regression routine into the uncertainty limits of each varied model parameter. These uncertainties also reflect possible correlation between parameters. The highest error for a time slice was  $\pm 0.002$  for the adsorbate fraction parameter. Using Eq. (2), one finds that this value translates to  $\pm 0.3$  mg/m<sup>2</sup>.

GE shows sensitivity to changes in the birefringence of anisotropic materials, caused in this case by the uptake of organic adsorbate. A chemically functionalized SCTF with binding selectivity to specific analytes could be used as a chemical sensor. When an analyte adsorption process is measured and analyzed by GE, the presence, amount of adsorption, and rate of adsorption can be determined.

## 5. Conclusion

In summary, we have demonstrated the dynamic, *in-situ* quantification of FN that adsorbs into the void spaces of SCTFs by GE. The optical model comprised an AB-EMA to describe the constituent materials' volumetric fractions within the SCTF while solvent and FN were exchanged during adsorption and rinsing processes. We discussed GE data modeling for *in-situ* measurements of optically anisotropic SCTFs for the specific application of organic molecule adsorption. An independent, simultaneous mechanical technique, QCM-D, was also employed to observe FN adsorption and rinsing. GE and QCM-D yielded qualitatively similar results for FN adsorption and rinsing. The quantitative QCM-D results are more difficult to interpret

because the SCTF might not be accurately described by the Sauerbrey equation.

### **Acknowledgments**

The authors acknowledge financial support from The Procter & Gamble Company, J.A. Woollam Co., Inc., the American Heart Association, the National Science Foundation under award numbers EPS-1004094 and ECCS-0846329, and the University of Nebraska-Lincoln College of Engineering. We gratefully acknowledge discussions with Mark Solinsky (The Procter & Gamble Company) and Tom E. Tiwald (J.A. Woollam Co., Inc.).